

Highly Improved Electrochemical Reactions of Mesoporous Carbon Electrodes in Electrochemical Energy Storage and Conversion

Si-Jin Kim,¹ Young-Woo Lee,¹ Sang-Beom Han,¹ Seong-Bae Kim,^{1,2} Woo-Seong Kim,²
Kyung-Won Park^{1,*}

¹ Department of Chemical Engineering, Soongsil University, Seoul 156-743, Republic of Korea

² Daejung Energy Materials, 740-49, Sinheung-dong, Iksan, Jeonbuk 570-140, Republic of Korea

*E-mail: kwpark@ssu.ac.kr

Received: 16 January 2013 / Accepted: 8 February 2013 / Published: 1 March 2013

We report mesoporous carbon electrodes prepared using silica template, carbonization process under CH₄ atmosphere, and subsequent silica removal for improved electrochemical energy storage and conversion in lithium-ion batteries, capacitors, and fuel cells. The as-synthesized carbon electrodes exhibit mesoporous structures with the narrow size distributions corresponding to the replication of the mesoporous SiO₂ template. In particular, the meso-C-3 prepared by carbonization process under CH₄ atmosphere for 3 h exhibits relatively much higher surface area of 635.07 m² g⁻¹ and pore diameter of ~3.13 nm with the narrow size distribution corresponding to the replication of the meso-SiO₂. The meso-C-3 shows high charge capacity and high-rate performance during the Li intercalation due to relatively high surface areas and well-defined pores as a buffer to the local volume changes. The improved electrochemical double layer capacitance and oxygen reduction reaction activity of the meso-C-3 might be due to large accessible surface area and pore structure in the well-defined porous electrode.

Keywords: Mesoporous; Carbon; Li intercalation; Capacitance; Oxygen reduction reaction

1. INTRODUCTION

Mesoporous carbons have attracted considerable attention because of their use as catalyst supports, adsorbents for bulky pollutants, as well as for electrode materials [1]. The mesoporous carbon materials have large surface area, large pore volume, and narrow pore size distribution. To prepare mesoporous carbon materials, there are several representative methods such as catalytic activation in the presence of certain metals, carbonization of polymer aerogels, carbonization of

polymer blends, and templating methods [2-4]. Especially, Santa Barbara-15 (SBA-15) silica templates synthesized using pluronic P123 triblock copolymer due to controllable pore sizes, specific surface areas, and pore volumes can provide mesoporous carbon for efficient electrochemical reactions in batteries, supercapacitors, and fuel cells [5,6].

For lithium-ion batteries (LIBs), graphite with limited storage capacity of 372 mAh g⁻¹ has been typically used as an anode because of its low cost and low electrochemical potential with respect to lithium metal [8,9]. However, storage capacity and rate performance of graphite anode materials should be essentially improved in order to achieve high-rate capability in LIBs. Since the diffusion of lithium ions in the bulk electrode is the rate-determining step, a variety of porous structures are promising for an excellent performance [10,11]. In general, since the capacitance in supercapacitors is dependent on the specific surface area of the electrode, porous carbon is used as an electrode material for supercapacitors because of its stable physical and chemical properties, large specific surface area, controlled pore structure, high conductivity, low cost, and availability [12,13]. The oxygen reduction reaction (ORR) plays a significant role in controlling the performance of the cathode in fuel cells, and efficient ORR electrocatalysts are essential for the practical applications of the fuel cells. The reduction of oxygen at carbon based electrodes has been extensively studied [14-16].

Herein, we prepared mesoporous carbon materials for electrochemical reactions by means of modified silica template method. The structural characterization of mesoporous carbon electrodes was carried out using field emission scanning electron microscopy (FE-SEM), field emission transmission electron microscopy (FE-TEM), small-angle X-ray diffraction (SA-XRD), and wide-angle X-ray diffraction (WA-XRD). The surface area and porosity of the electrodes were analyzed by a nitrogen sorption measurement. To evaluate the performance of the electrodes for electrochemical reactions, charge-discharge characteristics, electrochemical double layer capacitance, and ORR activity of the cathode materials were measured using a lithium coin cell and electrochemical cells, respectively.

2. EXPERIMENTAL

SBA-15 silica templates were synthesized using pluronic P123 triblock copolymer (EO₂₀PO₇₀EO₂₀). The pluronic P123 (4.0 g) was dissolved in 30 g of water and 120 g of 2 M HCl solution. Then, tetraethyl orthosilicate (TEOS, 8.50 g) was added, and the resulting mixture was stirred for 5 min and then kept at 35 °C for 20 h without stirring. This low-temperature preparation was loaded into a Teflon-lined stainless steel autoclave and heated at 100 °C for 72 h. Then, the powders obtained were collected and washed repeatedly with distilled water to remove any possible residual reactant. To completely remove the surfactant dried in an oven at 60 °C, and subsequently calcined at 600 °C in air for 4 h. The SiO₂ powders were put into a quartz tube under the flow of methane gas. The flow rate of N₂ gas (99.99%) was kept for 15 min to get rid of O₂ inside the tube. Under CH₄ flow rate of 100 mL min⁻¹, the furnace was heated at 900 °C for 3 or 5 h and then cooled down to 25 °C under methane atmosphere. The silica was removed with 1 M HF solution at 25 °C for 24 h, washed with water, and then dried at 60 °C oven.

The size and shape of the electrodes were observed using FE-SEM (JSM-6700F, Eindhoven,

Netherlands) and FE-TEM (Tecnai G2 F30 system operating at 300 kV). Nitrogen adsorption and desorption isotherms were measured at 77 K using a Micromeritics ASAP 2020. Before the adsorption measurements, all samples were outgassed at 473 K for 360 min in the port of the adsorption analyzer. The starting relative pressure was 0.995 P/P⁰ and ending relative pressure was 0.01 P/P⁰. Small-angle X-ray diffraction patterns were recorded on a small-angle X-ray diffractometer (SWXD, D/MAX-2500, Rigaku, Japan) using Cu K_α radiation (40 kV, 20 mA) at a scan rate of 1.0° min⁻¹ over the range of 0.25-6.0°. Wide-angle X-ray diffraction patterns were recorded using a Rigaku diffractometer equipped with a Cu K_α radiation source of λ = 0.15418 nm with a Ni filter. The tube current was 100 mA with a tube voltage of 40 kV. The 2θ between 10° and 80° was explored at a scan rate of 5.0° min⁻¹.

To assemble lithium coin cells (size 2032, Hohsen Corporation), the electrodes were fabricated by mixing 85 wt% of carbon electrodes (hard carbon (Malvern Instruments Ltd.) and as-prepared carbon samples) with 10 wt% polyvinylidene difluoride (PVDF) binder (Alfa Aesar), and 5 wt% Ketjan black (Alfa Aesar) in 1-methyl-2-pyrrolidinone (NMP) solvent (Aldrich, 99%). The mixed slurries were cast onto a Cu foil current collector and dried in air at 100 °C for 12 h. The electrode with an area of 1.32 cm² was dried at 70 °C vacuum oven. The electrodes were evaluated with respect to a lithium foil (FMC Corporation) counter electrode. The coin cells were assembled inside an Ar-filled glove box (< 5 ppm, H₂O and O₂). The positive and negative electrodes of the cells were separated from one another by a porous polypropylene membrane (Wellcos) and an electrolyte solution consisting of 1.1 M LiPF₆ in ethylene carbonate: diethylcarbonate (1:1) solvent mixture (Techon Semichem).

The capacitances of the electrodes were measured using a three-electrode cell in 0.1 M NaOH at 25 °C using a potentiostat (Metrohm, Autolab). A Pt wire and Hg/HgO (in saturated NaOH) were used as counter and reference electrode, respectively. The glassy carbon electrode as a working electrode was polished with 1, 0.3, and 0.05 μm Al₂O₃ paste and then washed in deionized water. The ORR activity of the electrodes was measured in 0.1 M NaOH at 25 °C using a potentiostat (Metrohm, Autolab). The rotating disk electrode as a working electrode was polished with 1, 0.3, and 0.05 μm Al₂O₃ paste and then washed in deionized water. The slurries for electrochemical analysis were prepared by homogeneously mixing the nitride powders and 25 g L⁻¹ of PVDF in NMP solution. The electrodes were formed by dropping 0.7 μL of the slurry on the glassy carbon electrode and then dried at 50 °C oven.

3. RESULTS AND DISCUSSION

The silica template synthesized using pluronic P123 triblock copolymer for mesoporous carbon electrodes, as observed by FE-SEM and FE-TEM (Fig. 1(a)-(c)), exhibits tube-type mesoporous structure with a relatively uniform pore diameter of ~10.0 nm. The carbon electrodes were prepared by heating at 900 °C for 3 and 5 h under CH₄ atmosphere using mesoporous SiO₂ template (meso-SiO₂), followed by removing the meso-SiO₂ template. During the carbonization process, carbon layers were coated on the wall of the meso-SiO₂ as a function of reaction time. The FE-SEM and FE-TEM images

of carbon electrode prepared by carbonizing for 3 h (meso-C-3) using the meso-SiO₂ are indicated in Fig. 1(d)-(f). The carbon electrode without the template shows tube-type mesoporous structure with pore size of ~3.0 nm. This represents that carbon layers are well formed along the the meso-SiO₂, even followed by removing the template, maintaining the frame structure of the template without any serious collaption.

However, the electrode (meso-C-5) carbonized for 5 h using the meso-SiO₂ seems to be fully filled in the template by carbon as indicated in Fig. 1(g)-(i). It is likely that due to the longer duration of the carbonization, the meso-C-5 might have smaller pore size and less monodispersed pore structure as compared to the meso-C-3.

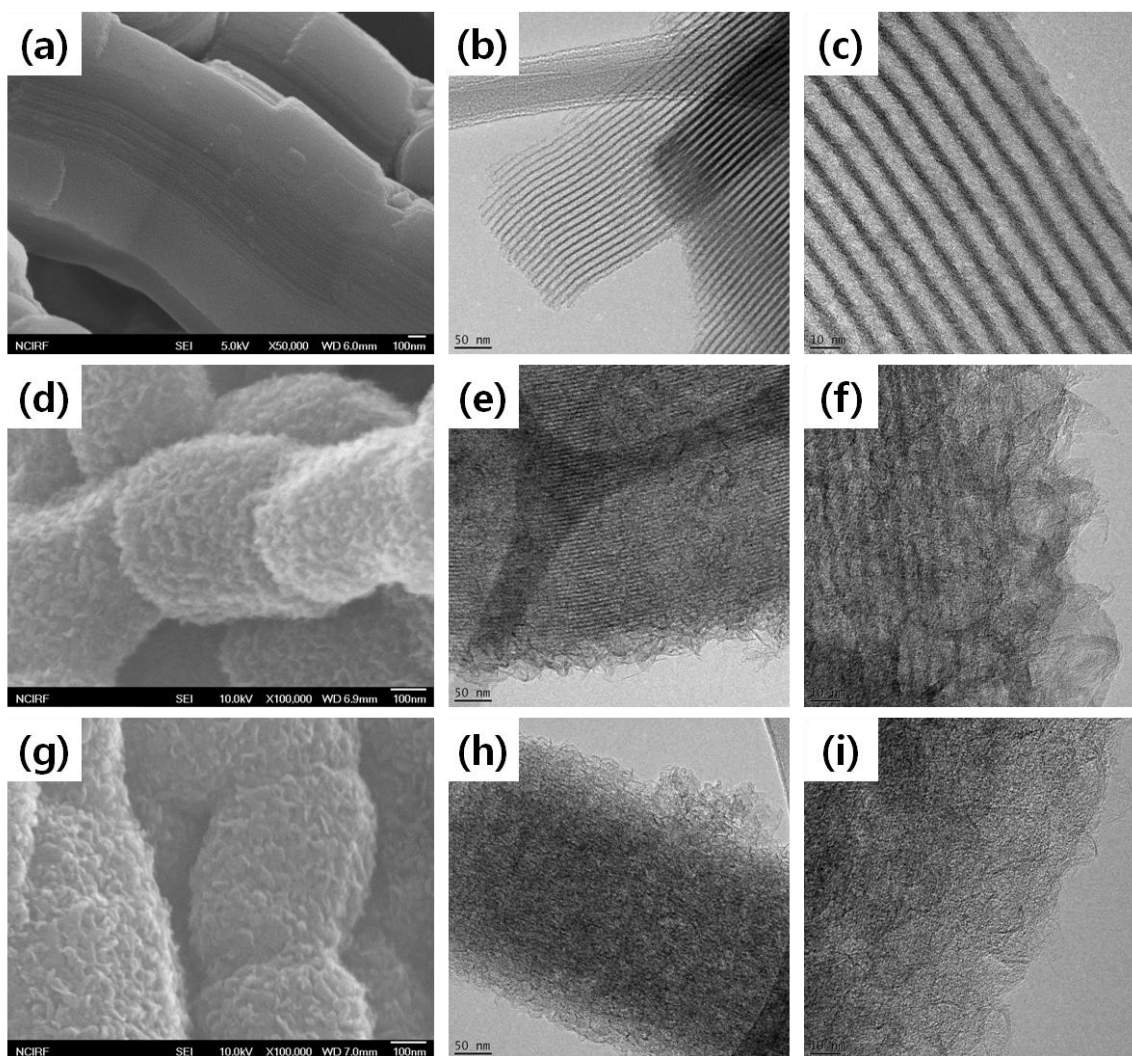


Figure 1. (a) FE-SEM image of meso-SiO₂; (b),(c) FE-TEM images of meso-SiO₂; (d) FE-SEM image of meso-C-3; (e),(f) FE-TEM images of meso-C-3; (g) FE-SEM image of meso-C-5; (h),(i) FE-TEM images of meso-C-5.

Fig. 2 shows nitrogen adsorption/desorption isotherms and pore size distribution curves of the meso-SiO₂, meso-C-3, and meso-C-5. All the isotherms of the samples are type IV hysteresis loops, indicating mesoporous structure, as shown in Fig. 2(a)-(c). The BET surface areas of the meso-SiO₂,

meso-C-3, and meso-C-5 are 838.97, 635.07, and 193.95 $\text{m}^2 \text{g}^{-1}$, respectively. The pore volumes of the meso-SiO₂, meso-C-3, and meso-C-5 are 1.20, 0.61, and 0.23 $\text{cm}^3 \text{g}^{-1}$, respectively.

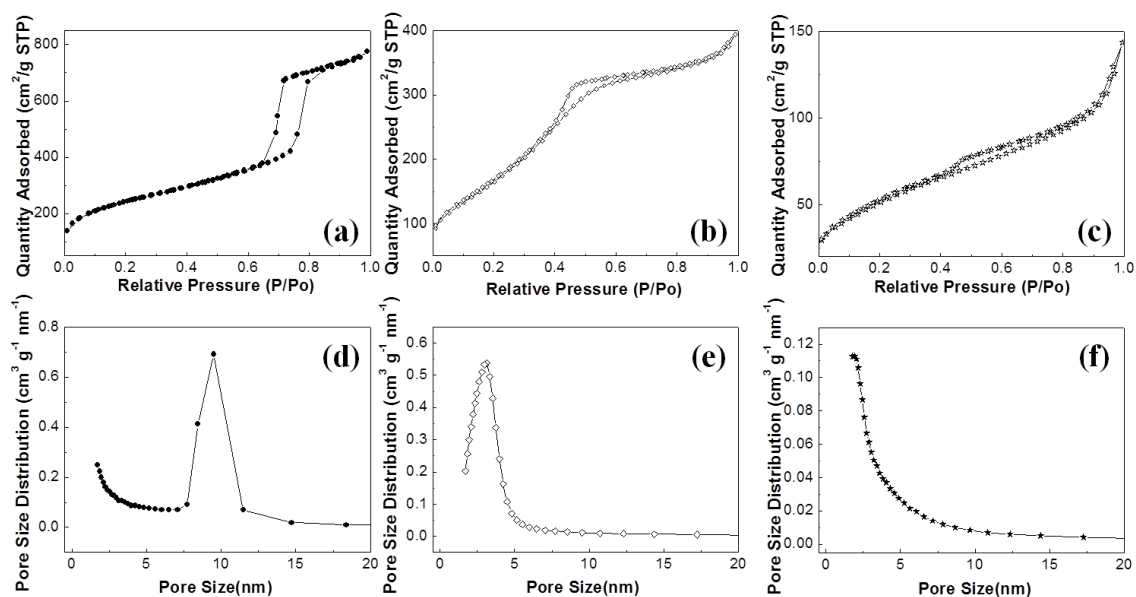


Figure 2. Nitrogen adsorption/desorption isotherms of (a) meso-SiO₂, (b) meso-C-3, and (c) meso-C-5 and pore size distributions of (d) meso-SiO₂, (e) meso-C-3, and (f) meso-C-5.

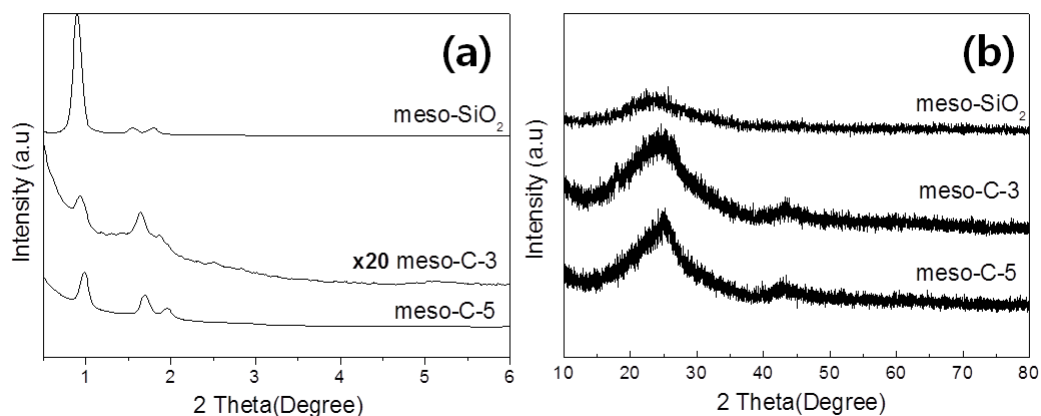


Figure 3. (a) SA-XRD and (b) WA-XRD patterns for meso-SiO₂, meso-C-3, and meso-C-5

The meso-SiO₂ as a template has an average mesopore diameter of ~9.47 nm with narrow size distribution in good agreement with TEM data (Fig. 2(d)). The pore size distribution curve of the meso-C-3 exhibits a mesopore with the pore diameter of ~3.13 nm with the narrow size distribution corresponding to the replication of the meso-SiO₂ (Fig. 2(e)). However, the meso-C-5 formed by the carbonization process for the longer reaction time has smaller pore diameter of ~2.09 nm with decreased surface area and pore volume in comparison with the meso-C-3 (Fig. 2(f)). This suggests

that the increased reaction time for the carbonization can lead to much thicker carbon layers of the inner meso-SiO₂. The well replication of the meso-C-3 and meso-C-5 from meso-SiO₂ as a template can be confirmed by SA-XRD patterns (Fig. 3(a)). Furthermore, the WA-XRD patterns of the meso-C-3 and meso-C-5 are shown in Fig. 3(b). The peaks for (002) and (101) planes of the meso-C-3 and meso-C-5 suggests that the carbon electrodes consist of graphitic carbon framework.

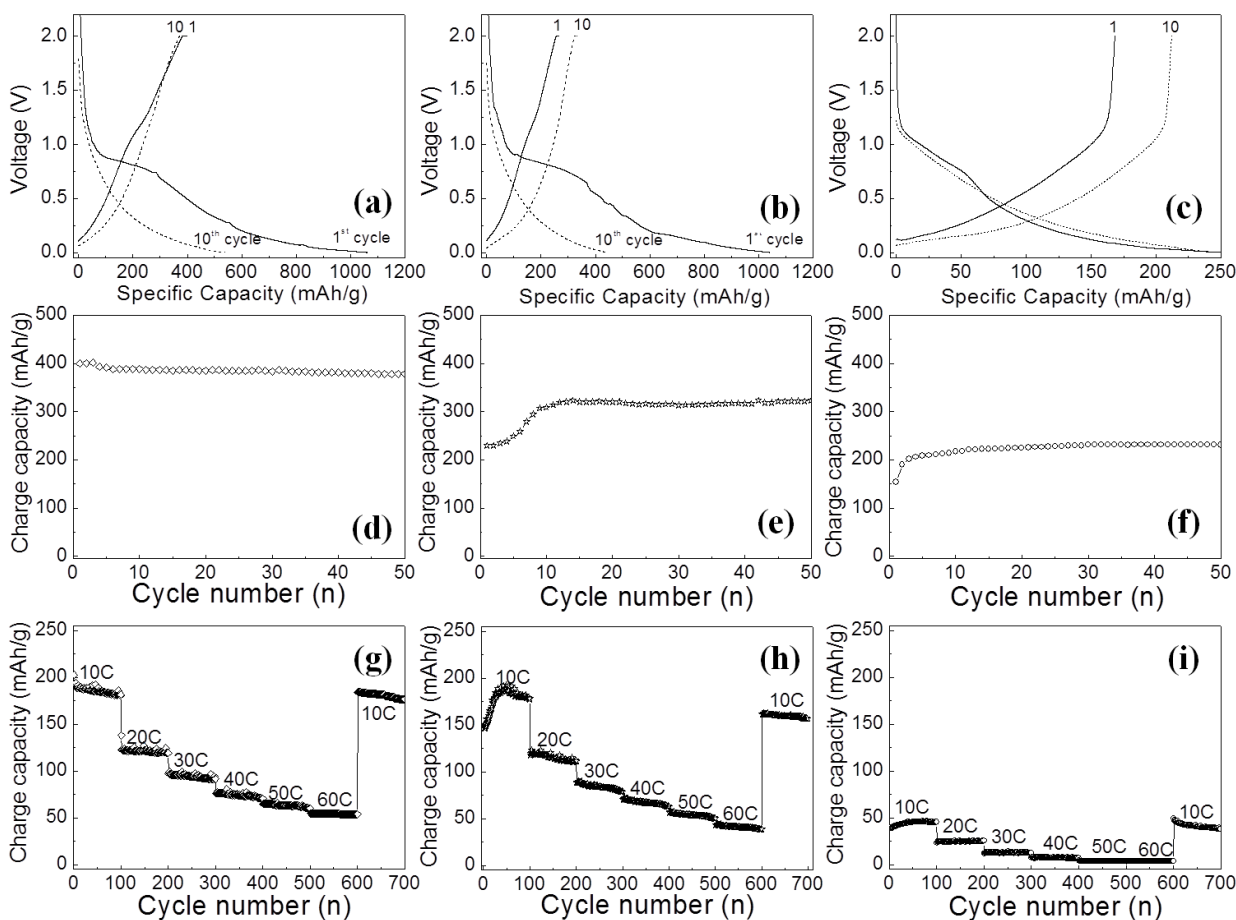


Figure 4. Charge-discharge curves of (a) meso-C-3, (b) meso-C-5, and (c) hard-C at 0.1 C. Cycling performance of carbon samples (d) meso-C-3, (e) meso-C-5, and (f) hard-C at 0.1 C for 50 cycles. Rate cycling performance of (g) meso-C-3, (h) meso-C-5, and (i) hard-C.

Fig. 4(a)-(c) shows discharge-charge curves of the mesoporous carbon electrodes for the first cycles at a rate of 0.1 C as compared to hard carbon (hard-C). At the cycling rate of 0.1 C, the first charge capacities of the meso-C-3, meso-C-5, and hard-C are 406, 232, and 168 mAh g⁻¹, respectively. As indicated in the of Fig. 4(d), the charge capacity of the meso-C-3 stabilizes after first cycle to ~400 mAh g⁻¹ for 50 cycles. As can be seen in the Fig. 4(e) and (f), the charge capacity of the meso-C-5 and hard-C stabilize after over 15 cycles to ~300 and ~200 mAh g⁻¹, respectively. Typically, although the irreversible capacity loss could originate from the reduction of the electrolyte resulting in the formation of a solid electrolyte interphase on relatively large specific surface of the samples, the meso-

C-3 exhibits less irreversibility and much higher capacity due to relatively favorable mesoporous structure for lithium ions mobility [17-19]. To investigate high-rate cycling performance of the electrodes, the discharge-charge rates were increased from 10 C to 60 C. As indicated in Fig. 4(g)-(i), the specific charge capacities of the meso-C-3, meso-C-5, and hard-C are 195, 148, and 45 mAh g⁻¹ at 10 C; 99, 85, and 12 mAh g⁻¹ at 30 C; 54, 41, and 8 mAh g⁻¹ at 60 C. The reversibility is demonstrated by the fact that the capacities of the meso-C-3, meso-C-5, and hard-C reach to 183, 161, and 48 mAh g⁻¹, respectively, once the rate is lowered to 10 C. The well-defined mesopores of the meso-C-3 and meso-C-5 may act as a buffer to the local volume changes during the Li insertion-extraction reactions, providing enough structural stability to the electrode and resulting in its better cycling stability compared to nonporous carbon electrode [20-24].

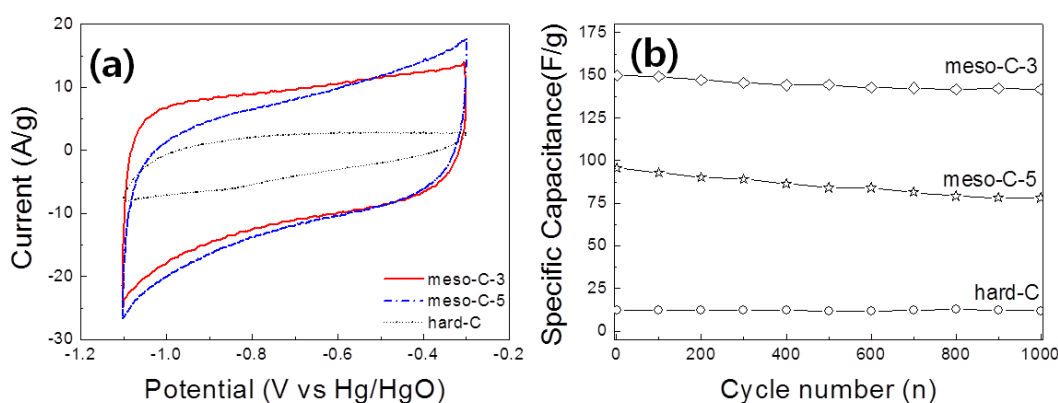


Figure 5. (a) CVs measured at a scan rate of 50 mV·s⁻¹ for meso-C-3, meso-C-5, and hard-C in 0.1 M NaOH. (b) Long-term cycling performance of the samples at a scan rate of 50 mV·s⁻¹ over 1000 cycles in 0.1 M NaOH.

Fig. 5(a) shows the CVs for the meso-C-3, meso-C-5, and hard-C in 0.1 M NaOH at a scan rate of 50 mV s⁻¹. No significant oxidation-reduction peaks are observed during the charge-discharge cycles representing that the charging-discharging is dominantly due to the double-layer mechanism. The specific capacitance obtained of the meso-C-3 (~151 F g⁻¹) is higher than those of the meso-C-5 (~95.9 F g⁻¹) and hard-C (~13 F g⁻¹). The cycling behavior for the electrodes is shown in Fig. 5(b) [25,26]. The meso-C-3 exhibits an excellent specific capacitance up to 1000 cycles, suggesting that the electrode is stable in 0.1 M NaOH within the potential window between -1.1 and -0.3 V. The improved capacitance of the meso-C-3 might be attributed to large accessible surface areas and pore structure [27].

To characterize ORR properties of the meso-C-3, meso-C-5, and hard-C in alkaline solution, CVs of the electrodes in 0.1 M NaOH were obtained as shown in Fig. 6(a)-(c). The onset potentials of ORR catalytic activity of the meso-C-3, meso-C-5, and hard-C in O₂-saturated 0.1 M NaOH are -0.08, -0.09, and -0.08 V, respectively, which might be similar within experimental uncertainties. Fig. 6(d) compares the ORR for the meso-C-3, meso-C-5, and hard-C in O₂-saturated 0.1 M NaOH at 25 °C at a rotation rate of 1600 rpm and a scan rate of 5 mV s⁻¹. The ORR activity of the meso-C-3 exhibits the

highest half-wave potential (~ -0.25 V) as compared to the meso-C-5 and hard-C. The value for the meso-C-3 of -0.016 mA cm $^{-2}$ at -0.145 V, near the kinetically controlled potential in the ORR, exceeds those for the meso-C-5 and hard-C. Furthermore, the high limiting current density of the meso-C-3 may result from efficient oxygen diffusion into the well-defined porous electrode as already described in the BET data [28,29].

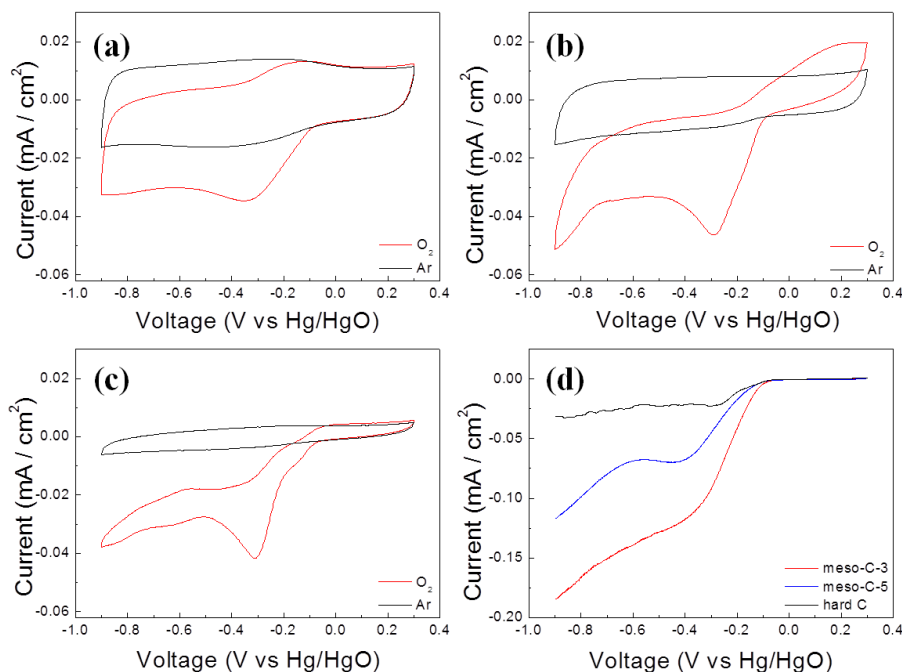


Figure 6. CVs of (a) meso-C-3, (b) meso-C-5, and (c) hard-C at a scan rate of 5 mV \cdot s $^{-1}$ and rotation disk speed of 1600 rpm in 0.1 M NaOH. (d) Polarization curves for ORR activity of the samples in O $_2$ -saturated 0.1 M NaOH.

4. CONCLUSIONS

We have prepared mesoporous carbon electrodes for highly improved electrochemical reactions using modified silica template and carbonization process. The as-prepared carbons exhibited well-defined mesoporous structure and relatively high surface area. The mesoporous carbon electrodes displayed superior Li intercalation properties to hard-C, facilitating lithium ion motion in the mesoporous electrodes as compared to the nonporous carbon. The improved capacitance of the meso-C-3 caused by the double-layer mechanism might be attributed to large accessible surface areas and pore structure. The excellent ORR activity of the meso-C-3 may result from efficient oxygen diffusion into the well-defined porous electrode.

ACKNOWLEDGMENTS

This work was supported by the IT R&D program of MKE/KEIT [KI002176, Development of 3.6Ah Class Cylindrical Type Lithium Secondary Battery] and the Human Resources Development of the

Korea Institute of Energy Technology Evaluation and Planning (KETEP) grant funded by the Ministry of Knowledge Economy, Republic of Korea (No. 20124030200070).

References

1. Y.-S. Hu, P. Adelhelm, B. M. Smarsly, S. Hore and M. Antonietti, *Adv. Funct. Mater.*, 17 (2007) 1873.
2. M. Kruk, M. Jaroniec, R. Ryoo and S.H. Joo, *J. Phys. Chem. B*, 104 (2000) 7960.
3. S. Jun, S. H. Joo, R. Ryoo, M. Kruk, M. Jaroniec, Z. Liu, T. Ohsuna and O. Terasaki, *J. Am. Chem. Soc.*, 122 (2000) 10712.
4. J. Kim, J. Lee and T. Hyeon, *Carbon*, 42 (2004) 2711.
5. M.-S. Kim, B. Fang, J. H. Kim, D. Yang, Y. K. Kim, T.-S. Bae and J.-S. Yu, *J. Mater. Chem.*, 21 (2011) 19362.
6. T. Zheng, Y. Liu, E.W. Fuller, S. Tseng, U. Von Sacken and J. R. Dahn, *J. Electrochem. Soc.*, 142 (1995) 2581.
7. F. Lufrano and P. Staiti, *Int. J. Electrochem. Sci.*, 5 (2010) 903
8. A.S. Aricò, P. Bruce, B. Scrosati, J.-M. Tarascon and W.V. Schalkwijk, *Nature Mater.*, 4 (2005) 366.
9. F. Bonino, S. Brutti, P. Reale, B. Scrosati, L. Gherghel, J. Wu and K. Müllen, *Adv. Mater.*, 17 (2005) 743.
10. J. R. Dahn, T. Zheng, Y. Liu and J.S. Xue, *Science*, 270 (1995) 590.
11. M. Winter, J.O. Besenhard, M.E. Spahr and P. Novák, *Adv. Mater.*, 10 (1998) 725.
12. K. Lee, L. Zhang, H. Lui, L. Hui, Z. Shi and J. Zhang, *Electrochim. Acta*, 54 (2009) 4704.
13. Y. Zhai, Y. Dou, D. Zhao, P.F. Fulvio, R.T. Mayes and S. Dai, *Adv. Mater.*, 23 (2011) 4828.
14. K.J.J. Mayrhofer, D. Strmcnik, B.B. Blizanac, V. Stamenkovic, M. Arenz and N.M. Markovic, *Electrochim. Acta*, 53 (2008) 3181.
15. H.A. Gasteiger, J.E. Panels and S.G. Yan, *J. Power Sources*, 127 (2004) 162.
16. V. Nallathambi, J.-W. Lee, S.P. Kumaraguru, G. Wu and B.N. Popov, *J. Power Sources*, 183 (2008) 34.
17. S. Wang, S. Yata, J. Nagano, Y. Okano, H. Kinoshita, H. Kikuta and T. Yamabe, *J. Electrochem. Soc.*, 147 (2000) 2498.
18. T. Zheng, W.R. McKinnon and J.R. Dahn, *J. Electrochem. Soc.*, 143 (1996) 2137.
19. K. Zaghib, F. Brochu, A. Guerfi and K. Kinoshita, *J. Power Sources*, 103 (2001) 140.
20. M. Herstedt, L. Fransson and K. Edström, *J. Power Sources*, 124 (2003) 191.
21. H. Habazaki, M. Kiriou and H. Konno, *Electrochem. Commun.*, 8 (2006) 1275.
22. S. Ahn, Y. Kim, K.J. Kim, T.H. Kim, H. Lee and M.H. Kim, *J. Power Sources*, 81-82 (1999) 896.
23. H.-C. Shin, M. Liu, B. Sadanadan and A.M. Rao, *J. Solid State Electrochem.*, 8 (2004) 908.
24. F. Zhang, K.-X. Wang and G.-D. Li, *Electrochem. Commun.*, 11 (2009) 130.
25. E. Frackowiaka and F. Beguin, *Carbon*, 39 (2001) 937.
26. X. Zhai, J. Liu, P. Liu, M. Zhong, C. Ma, H. Wang, Q. Guo, Y. Song and L. Zhi, *Int. J. Electrochem. Sci.*, 7 (2012) 7304.
27. E. Frackowiaka and F. Beguin, *Carbon*, 40 (2002) 1775.
28. R. Chen, H. Li, D. Chu and G. Wang, *J. Phys. Chem., C* 113 (2009) 20689.
29. G. Jürmann, D.J. Schiffrin and K. Tammeveski, *Electrochim. Acta*, 53 (2007) 390.